Applied Physics A (2023) 129:361
https://doi.org/10.1007/s00339-023-06638-6

Applied Physics A
Materials Science & Processing

Effect of germanium alloying on microstructure and properties of Ti-6Al-4V alloy fabricated by additive manufacturing

Changfu Li[1] · Jiaqi Bu[1] · Xiangming Wang[2] · Guang Yang[1]

Received: 31 January 2023 / Accepted: 10 April 2023 / Published online: 18 April 2023

Abstract

The microstructure of Ti-6Al-4V titanium alloy produced by laser additive manufacturing is generally relatively coarse, so its mechanical properties have not yet achieved satisfactory results. After adding germanium element to titanium alloy, second phase particles can be formed, at the same time, due to strong bonding force between Ti and Ge atoms, there also have other strengthening effects that need to be revealed. Therefore, the effect of Ge addition on the microstructure and mechanical properties of additive manufactured Ti-6Al-4V alloy was studied in detail in this paper, which can provide more reference for optimizing the performance of titanium alloy manufactured with additives manufacturing. The pure Ge powder was ball milled with Ti-6Al-4V powder in several different proportions, and bulk samples were prepared by laser deposition manufacturing (LDM) with the mixed powder. The Germanium alloyed Ti-6Al-4V alloy's tensile strength and plasticity at room temperature increased about 25% and 10%, respectively, compared with LDMed Ti-6Al-4V alloy without Ge. According to the results of TEM and EDS, Ti and Ge reacted to form granular second phase Ti_5Ge_3, which distributes along the primary β grain boundary inhibit the growth of columnar crystals. Part of Ge solutes into α phase. Both microstructure refinement and solid solution are very effective in impeding the moving of dislocation, so that the Germanium alloyed LDMed Ti-6Al-4V alloy showed excellent tensile property at room temperature.

Keywords Laser deposition manufacturing · Titanium alloy · Short-range order · Microstructure · Mechanical properties

1 Introduction

With the increasing demand for titanium alloys, Laser Deposition Manufactured (LDM) Ti-6Al-4V titanium alloys draw more and more attention. Compared with the traditional forming methods, such as casting, forging, and welding [1–3], LDM technology have obvious advantages in forming efficiency, structure performance, and manufacture cost. Currently, some mechanical properties of Ti-6Al-4 V alloy prepared by LDM technology have reached or even exceeded those of the forged. However, due to the high density energy input and the rapid cooling, coarse columnar crystals form easily in the alloy. The fabricated parts exhibit obvious anisotropy, as well as the toughness and fatigue properties need to be improved [4, 5]. To adjust and control the microstructure and improve the mechanical properties of Ti-6Al-4 V alloy prepared by additive manufacturing, appropriate technological methods have to be carried out [6, 7].

Because of the unique microstructure and mechanical properties of the Ti-6Al-4V titanium alloy prepared by the LDM process, the preparation technology, post-heat treatment, and addition of borides and rare earth elements were investigated to improve its structure and properties [8–13]. Although optimizing LDM process parameters and post-heat treatment have effect on microstructure and property adjustment, the results are limited [8, 9]. Addition of borides, rare earth elements can effectively control the size of the columnar crystal, as the second phase particles in micron or nanometer size can act as condensation nucleus. The strength of the matrix itself has not been improved, and it is easy to reduce the plasticity and toughness of the material [10–13], the mechanical properties of the alloy at high temperatures may be impaired. Therefore, the method of

✉ Changfu Li
20140029@sau.edu.cn

[1] Key Laboratory of Fundamental Science for National Defence of Aeronautical Digital Manufacturing Process, Shenyang Aerospace University Shenyang Liaoning, Shenyang 110136, China

[2] Shenyang Aircraft Design Institute of AVIC, Shenyang 110035, Liaoning, China

performance enhancement of additive manufacturing titanium alloy requires more extensive and in-depth research.

Adding or increasing specific solute atoms to metals solid solution can improve their elastic limit, yield strength, and high-temperature strength of the material [14–18]. Hu Qingmiao et al. [19] discovered that elements such as Al, Ga, Ge, and Si promote the formation of ordered phases in titanium alloys. Al and Ga elements are generally used as α stable elements. Si tends to form silicide particles, which acts as the second phase to reinforce the metal matrix [20, 21]. Ge has relatively higher solubility in α-Ti than Si, and Ge–Ti has higher bonding tendency than Al–Ti and Ga–Ti [22] and may form new solid solutions based on α-Ti[19]. The titanium alloy with Ge addition has good comprehensive mechanical properties under the traditional process [23, 24], while seldom reports were made on the microstructure and properties of Ge alloyed Ti-6Al-4V titanium alloy made by LDM. In present research, the microstructure and mechanical properties of Ti-6Al-4 V alloy manufactured by LDM with different Ge contents were investigated, and the mechanism of Ge in microstructure formation and performance strengthening was discussed.

2 Experimental

As shown in Fig. 1a, the LDM experiment was performed on an LDM-800 laser deposition manufacturing system outfitted with a IPG 6000W fiber laser, powder feeding system with four coaxial nozzles, environmental control system, monitoring, and feedback control system, and so on. The moving range of the executive system on the three axes of XYZ is 800 mm, 800 mm and 600 mm, respectively.

The deposition substrate was a forged Ti-6Al-4V titanium alloy plate with a thickness of 40 mm, and the Ti-6Al-4V powder with a particle size of 45 μm–180 μm was prepared using the plasma rotary electrode method. High purity Ge powder with a particle size of 30–150 μm was ball-milled with Ti-6Al-4V powder with mass percentage of 0%, 1%, 2%, 3%, 4%, and 5%, respectively, and the ball milling process was conducted on a YXQM planetary ball mill with following parameters, zirconia ball with diameter of 3 mm, ball to powder ratio of 5:1, ball milling speed of 230 rpm. Six groups of mixed powders were obtained, each with a mass of 400 g. Before deposition, each group of Ti-6Al-4V powder was dried at 120 °C for 8 h, and the surface of the substrate to be deposited was mechanically ground into a fresh surface.

The LDM process parameters are laser power at 1.8 kW, scanning rate at 8 mm/s, scanning interval at 2 mm, and layer thickness at 0.5 mm. The dimensions of the sample in *X*, *Y*, and *Z* directions are 45 mm × 15 mm × 65 mm in design, respectively. The schematic diagram of sample forming dimensions is shown in Fig. 1b. Plate-shaped tensile samples were cut and prepared along the parallel substrate plane (XY plane) at a position more than 5 mm away from the substrate plane. The gauge section is 15 mm × 3 mm, and the total length of the samples was 39 mm. Three plate-shaped tensile samples were available for each group of powder-deposited blocks, and 18 tensile samples were obtained in total.

The metallographic specimens corroded after mounting, pre-grinding, and polishing and the corrodent was Kroll corrosive agent ($HF–HNO_3–H_2O$ volume ratio is 1:2:17). Microstructure observation was performed at the GX51 OLYMPUS Optical Microscope (OM) and ZEISS ΣIGMA Scanning Electron Microscope (SEM). The parameters of SEM image are acceleration voltage of 15 kV, working distance of 10.3 mm and magnification of 5 k. The tensile tests were performed by INSTRON5982 electronic universal testing machine, displacement control is adopted during stretching, and the initial strain rate of the is 0.005 min^{-1}. Specimens were inspected using the Bruker D2 X-ray diffractometer (XRD) to determine the phase constitution.

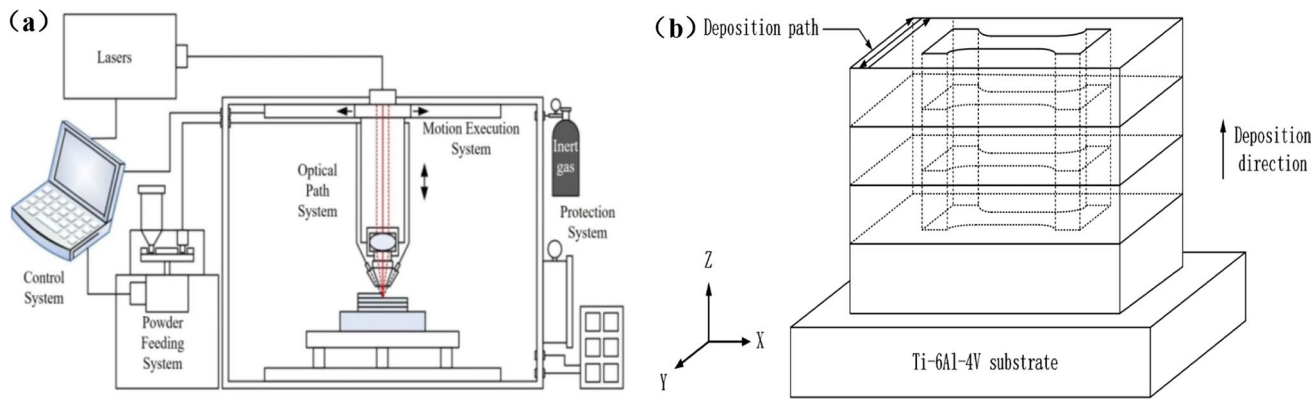

Fig. 1 **a** System schematic diagram of LDM-800, **b** Ti-6Al-4V deposition blocks with Ge content of 0–5% prepared by the LDM process

The fine structure of the alloy was analyzed under the field emission transmission electron microscope (TEM) of Talos F200X equipped with Oxford Xplore 30 EDS detection system.

3 Results

3.1 Phase identification

Figure 2 depicts the XRD spectrum of Ti-6Al-4V alloys prepared by the LDM process with varying Ge content. The diffraction peaks of α phase or β phase dominate in each spectral line, and the intensities of α phase and β phase diffraction peaks change with different Ge content.

As the Ge content rises above 3%, the diffraction peak of the second phase Ti_5Ge_3 in the spectral line becomes more visible. Among them, (111)Ti_5Ge_3 diffraction peak intensity changes the most. The XRD spectrum indicated that Ti and Ge in the alloy reacted under LDM process conditions, resulting in the formation of the second-phase Ti_5Ge_3.

3.2 Microstructure and morphology

Figure 3a shows the typical as-deposited microstructure of LDMed Ti-6Al-4V alloy observed along the direction perpendicular to the deposition direction (Z axis) in the absence of Ge addition. The primary β columnar grains is about 200 to 500 μm in diameter. The interior of β grain is composed of lamellae α, with residual β phases between α phases. The α lamellae took β grain boundaries as the initial point, and grew in a determined orientation into the grain in a bunched shape, with a single lamina width of about 1 ~ 1.5 μm, 10 ~ 25 μm in the length of and aspect ratio at about 13.

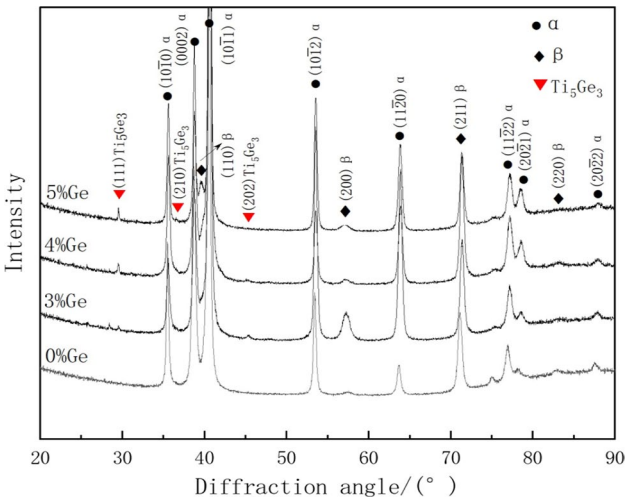

Fig. 2 XRD spectra of Ti-6Al-4V alloys prepared by the LDM process with different Ge content

The addition of 1% Ge to the alloy reduced the long axis size of the β column crystal slightly, but the morphology of the α layer inside the grain remained unchanged. When the Ge content reached 2%, the long axis of β columnar crystals decreased further. When Ge was added to 3%, the primary β grains appeared to be roughly equiaxed, as illustrated in Fig. 3b. It can be seen that the point-like precipitates distributed near the grain boundary, and the cluster structure around the grain boundary decreased. There are punctate precipitates in the grain as well, but their distribution density is lower than that near the grain boundary.

Figure 3c depicts the morphology of equiaxed grains at 4%Ge content. The primary *β* grains are completely equiaxed, and the grain size is smaller than in samples with lower Ge content. The density of the dot-like precipitated phase increased in the alloy, and the precipitation phase density near the grain boundary of the primary *β* crystal is greater than the intragranular density.

When the Ge content is 5%, the primary *β* grains remain equiaxed. As shown in Fig. 3d, the size did not change compared with the 4%Ge sample. The proportion of dot-like precipitated phase increases as the Ge content increases. It is still densely distributed along the grain boundary, but less within the grain, and the lamellar α has coarsened even more.

Figure 4 depicts the microstructure of alloys with different Ge content under SEM. With the increase of Ge content, the width of *α* lamellae in the primary β grain gradually increased and the long axis gradually shortened. The Image J image processing software was used to generate statistics on the size of lamellar α phases in the figure, and 50 *α* laminar were chosen in each alloy, and their length and width were measured manually. The variation of α laminar dimension is illustrated in Fig. 4f. As the Ge content increases, α lamellae become coarser and the aspect ratio decreases.

The width of the precipitated phase is generally about 0.3–1 μm, showing an irregular shape, mostly distributed at the interface between α and residual β phase under the SEM, as shown in Fig. 4. The EDS results show that the ratio of Ti element content to Ge element content (at%) in bulk precipitates is about 5:3. Combined with the XRD pattern (see Fig. 2), Ti_5Ge_3 can be determined.

3.3 Distribution of Ge element

Figure 5 illustrates the distribution of germanides and Ge elements in SEM morphology near the primary β grain boundary and within the primary β grain for the 4%Ge alloy. There are numerous dot-like germanides at the grain boundary, as shown in Fig. 5a. The distribution of germanides in the grain is dispersed, as depicted in Fig. 5c. Comparing

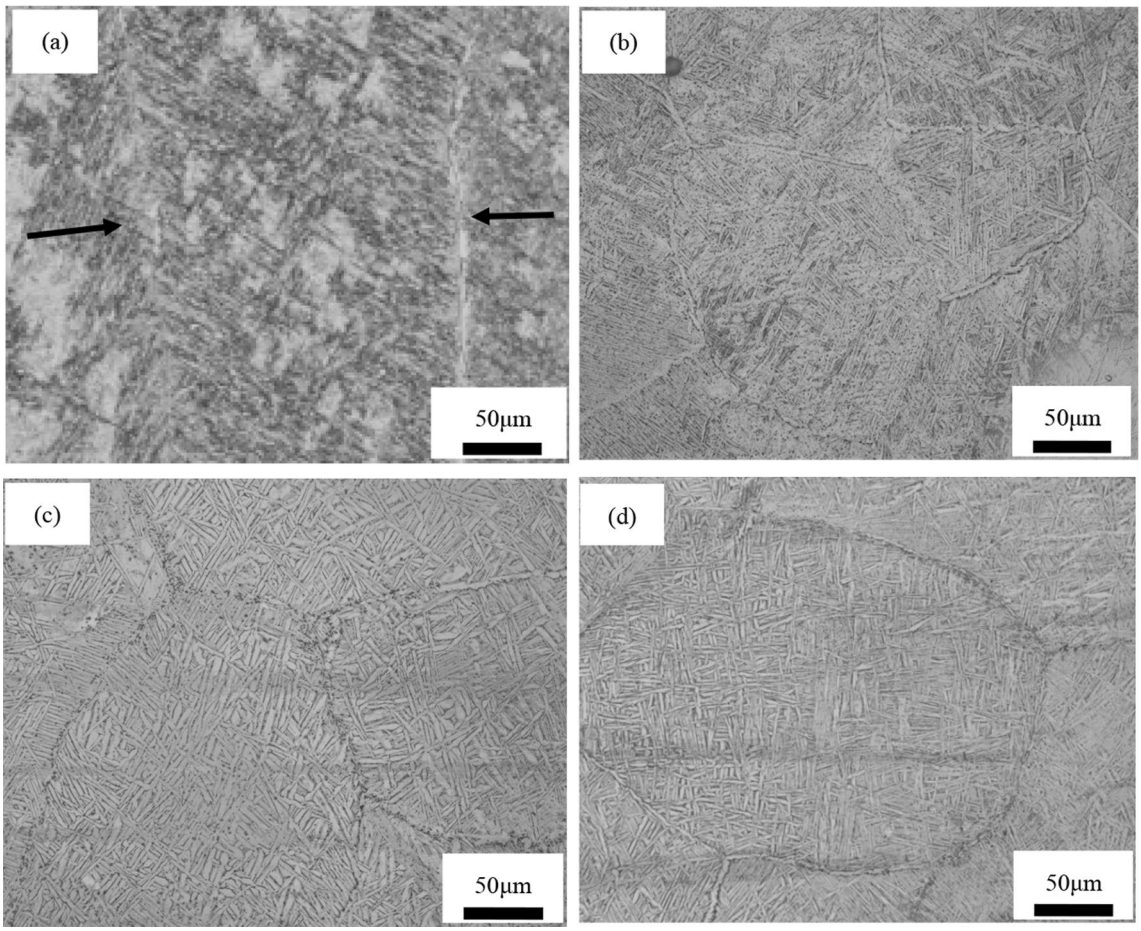

Fig. 3 Metallographic microstructure of Ti-6Al-4 V alloy with different Ge content prepared by LDM technology. (**a**) 0% Ge; (**b**) 3% Ge; (**c**) 4%Ge; (**d**) 5% Ge;

Fig. 5b and Fig. 5d, it can be seen that Ge exists mainly in form of the second phase, but a small part distributes in the α matrix.

The Ti_5Ge_3 is mainly concentrated at the primary β grain boundary, because when Ge and Ti react in situ in the laser molten pool, the formed Ti_5Ge_3 will solidify before the molten pool due to its higher melting point. Following this process, Ti_5Ge_3 acted as a heterogeneous nucleus particle, facilitating the heterogeneous nucleus progress in the molten pool. The appearance of Ti_5Ge_3 effectively inhibited the growth of coarse β columnar grain, and as the Ti_5Ge_3 ratio increased, the primary β grain morphology changed from columnar to equiaxed (see Fig. 3). The presence of Ti_5Ge_3 hampered the growth of β grain boundary, and Ti_5Ge_3 enrichment occurred at β grain boundary.

The EDS results performed at the "☆" and "□" area for quantifying in Fig. 5a, c and mapping in Fig. 5b, d show the Ge element distribution characteristics. There are apparent differences in the distribution of Ge elements at the primary β grain boundary and within β grain, as shown in Fig. 5b, , respectively. In Fig. 5b, the distribution contrast of Ge element in the second phase and the matrix is obvious, indicating that the majority of Ge elements exist as massive Ti_5Ge_3. While in Fig. 5d, although the contrast of bulk Ti_5Ge_3 is outstanding, the relative contrast of Ge element in the matrix increased, and the relative contrast difference between them is smaller than in Fig. 5b, which indicates that the matrix contains a certain amount of Ge element. There is a certain solid solubility for Ge in both β-Ti and α-Ti, but more in α-Ti. The EDS results that part of Ge element formed the second phase of Ti_5Ge_3, and the other Ge element dissolve into the matrix.

3.4 Tensile test

The tensile properties of as-deposited Ti-6Al-4V titanium alloys were tested at room temperature using the plate-like tensile parts shown in Fig. 1b. In addition, Fig. 6 is a comparison chart of tensile properties of each group of samples (the data in the chart was the arithmetic average of three samples in one group). The results show that Ge has a significant impact on the strength and plasticity of

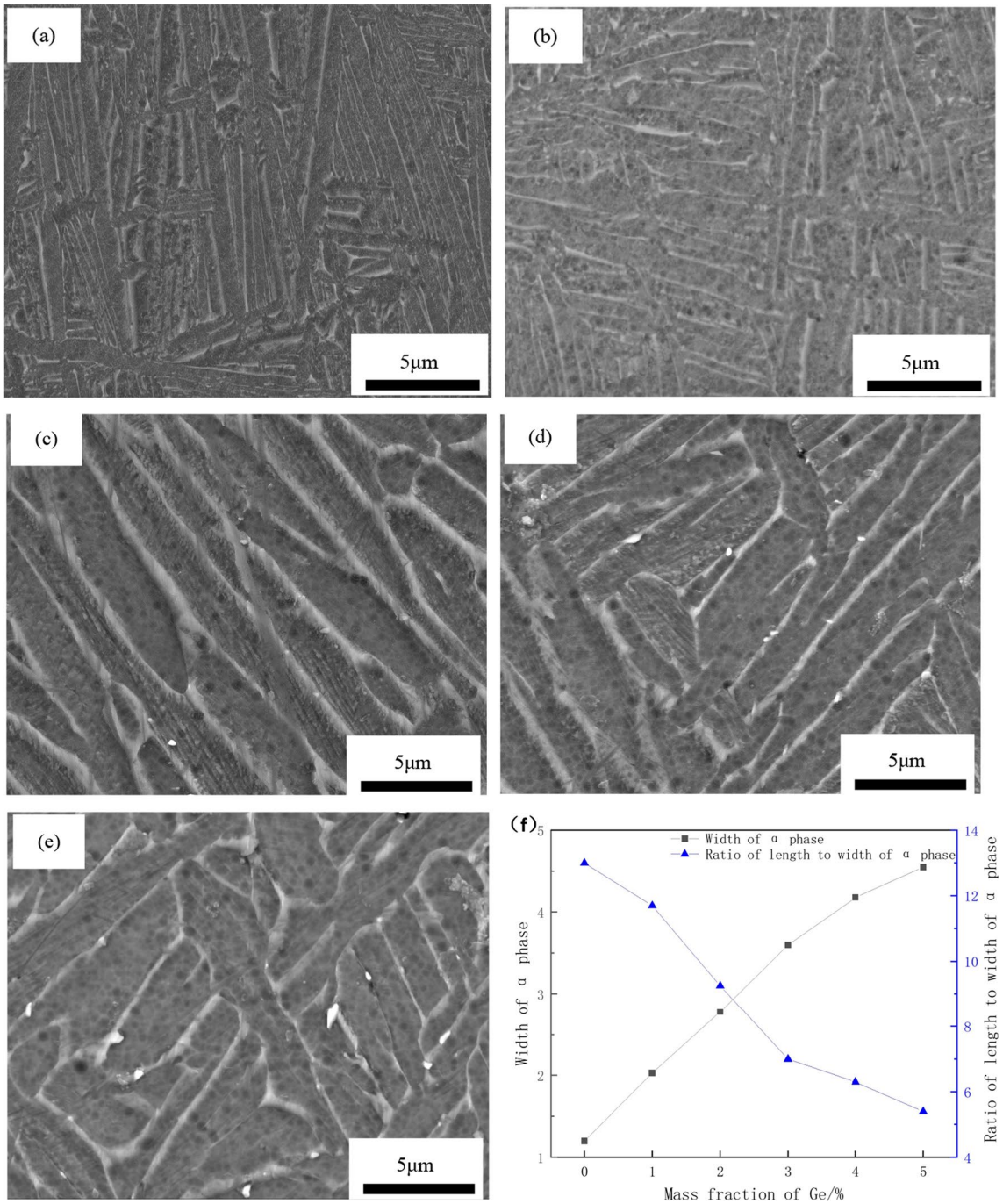

Fig. 4 Scanning electron microstructure of Ti-6Al-4V alloy with different Ge content prepared by LDM technology. (**a**) 0% Ge; (**b**) 1% Ge; (**c**) 3%Ge; (**d**) 4% Ge; (**e**) 5% Ge; (**f**) The trend diagram of average width and aspect ratio of α lath with Ge content

LDMed Ti-6Al-4 V alloy, and the general trend of strength increases with increasing Ge content. When Ge content reaches 5%, the tensile strength, yield strength, and elongation increase by 28.7%, 22.4%, and 12.5%, respectively, compared with those without Ge.

4 Discussion

The microstructure and mechanical properties of Ti-6Al-4V alloy prepared by LDM changed noticeably with the

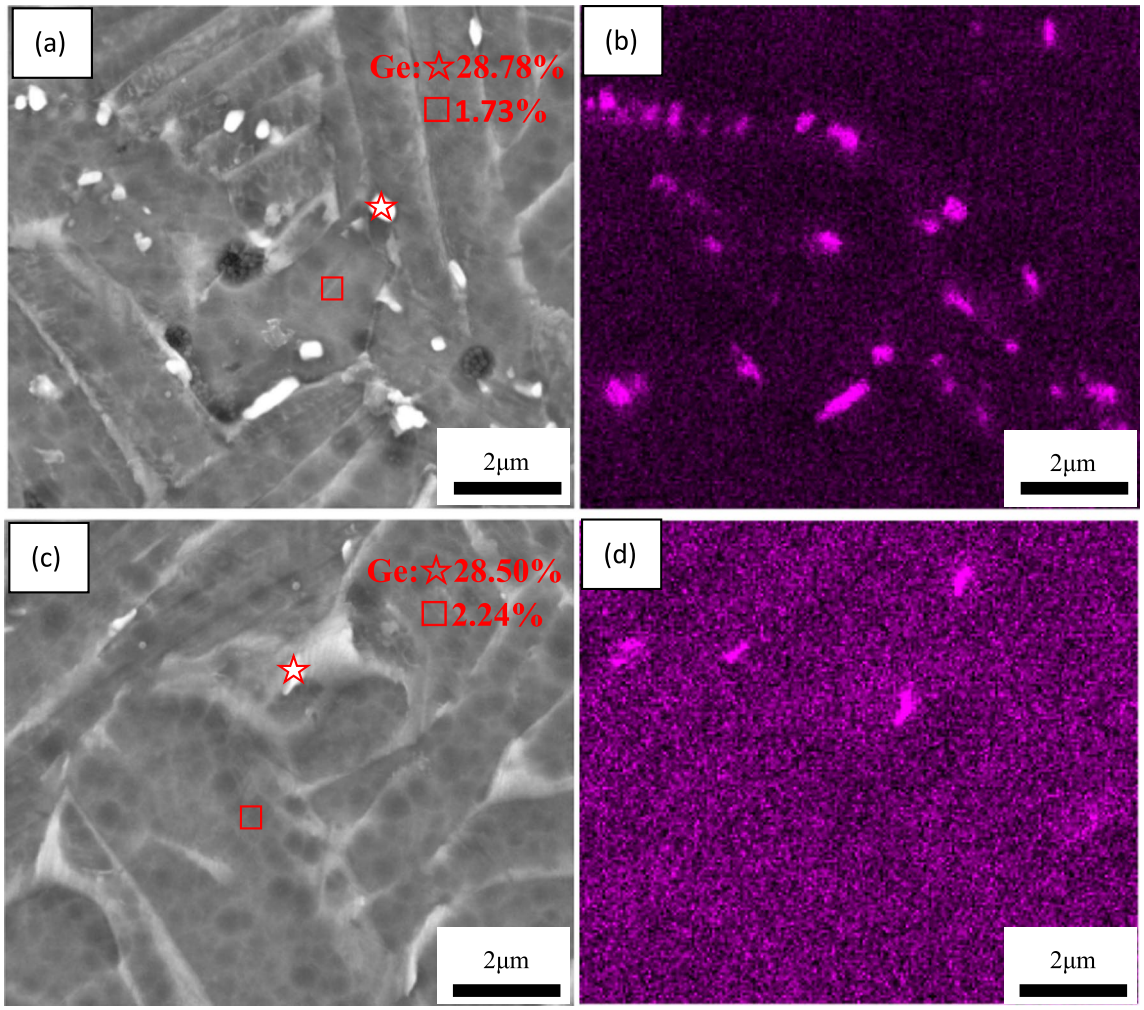

Fig. 5 SEM morphology of grain boundary and intragranular of as-deposited Ti-6Al-4V tensile sample containing 4%Ge, and distribution of Ge element. (**a**) at grain boundaries; (**b**) distribution of Ge element at grain boundaries; (**c**) within grains; (**d**) distribution of Ge element within grains

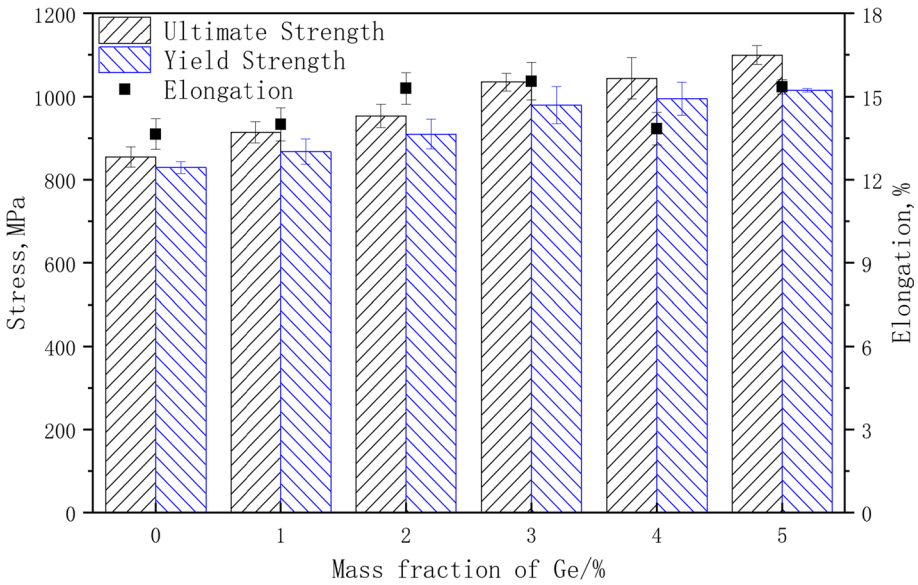

Fig. 6 Comparison diagram of tensile properties of Ti-6Al-4V alloy with different Ge content (0–5%) prepared by LDM

addition of Ge element, indicating that Ge alloying is a very effective method for LDMed Ti-6Al-4V alloy performance regulation. The mechanism of strengthening is discussed as follows.

After Ti-6Al-4V alloy powder doped with the Ge element, the Ge element would react with the Ti matrix during the formation of the molten pool. According to the experimental results shown in Figs. 2 and 6, the Ge element reacted with the matrix Ti in two states. In the first case, the Ti_5Ge_3 particles were formed, and it is beneficial to inhibit the growth of columnar crystals and promote the formation of equiaxed crystals. In the second case, Ge dissolved in the Ti matrix. Ge and Ti have a degree of solid solution because of their relatively strong bonding tendency, and Ge may affect the matrix lattice structure at the atomic level.

Selected area diffraction patterns (SADP) of α phase and Ti_5Ge_3 are shown in Fig. 7. In Fig. 7a, a massive Ti_5Ge_3 precipitate was surrounded by α lath. As TEM sampling position is close to the fracture of the tensile sample, a certain plastic deformation has also occurred at the location of the observation area. There are several dislocation queues in Fig. 7a, and it is worth noting that near the massive Ti_5Ge_3 precipitated phase, the dislocation was obvious pile-up and deflected. The above phenomenon shows that the existence of Ti_5Ge_3 effectively hinders the movement of dislocation and significantly changes α lath deformation process and plays a positive role in improving the strength of materials, i.e., hindering the grain sliding and dislocation movement [25].

Strength is the ability of materials to resist plastic deformation and fracture. A large number of studies [17, 26, 27] have shown that dislocation slip and twin deformation are the main deformation mechanisms that dominate the plastic behavior of materials. Zhang Ruopeng et al. [17] discovered that in the CrCoNi system, the random distribution of dislocations was observed in water-quenched samples without superlattice diffraction. In the SRO (Short-Range Ordering, SRO) sample, there was a significant local plane slip trajectory, and the leading dislocation tended to form a dislocation pair. The presence of a dislocation pair in a regularly arranged dislocation queue is widely regarded as a sign of ordered structure [19, 20, 26], the reason is that the initial dislocation's movement destroyed the SRO structure and resulted in the diffusion antiphase boundary (DAPB) behind the plane fault, while the sliding of the second dislocation almost offset the DAPB produced by the first dislocation due to the destruction of SRO. This energetic resistance is sufficient to inhibit the motion of a single dislocation, so at least two dislocations need to move in an interrelated manner to overcome the resistance of that fault [19]. The motion of the initial dislocation pair disrupts the SRO atomic structure and overcomes the energy barrier caused by the DAPB. Thereafter, dislocations will slide along the same path, experiencing a lower energy barrier.

In Fig. 8, a large number of neatly arranged dislocations in two queues were found in LDMed Ti-6Al-4V with 5%Ge, and the first two dislocations in the lower queue were paired. This may be the prove that Ge promotes ordering effect of α phase.

As an effective supplement to dislocation, twins are important deformation methods that can effectively enhance the deformation ability and strengthen the alloy. Kumar [28] investigated the relationship between super-lattice diffraction and the deformation mechanism, discovered that the emergence of deformed twins played a role in stress relief and improved the toughness of the alloy. As shown in Fig. 9, the specimen with 5% Ge is stretched at room temperature, and the interface structure of the deformed twin crystal is displayed in the alloy matrix.

Twinning and dislocation movement are coordinated with each other during metal materials' deformation process [29]. When a queue of dislocation forms, stress concentration

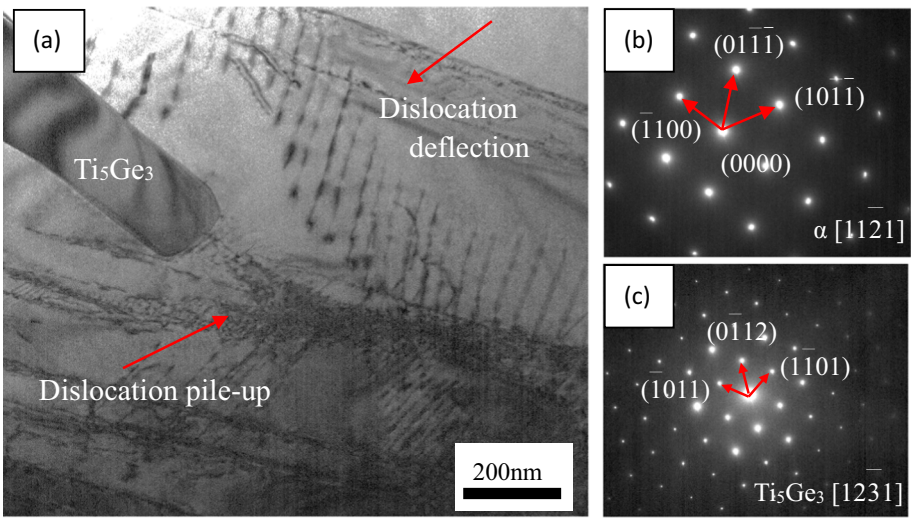

Fig. 7 **a** Bright field image of α matrix in 5% Ge sample with Ti_5Ge_3, (**b**) SADP of the matrix, (**c**) SADPs of Ti_5Ge_3

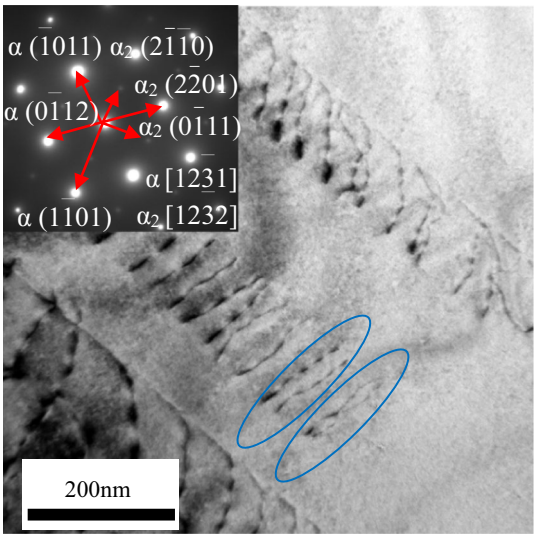

Fig. 8 Neatly arranged dislocation queues with paired initial dislocation

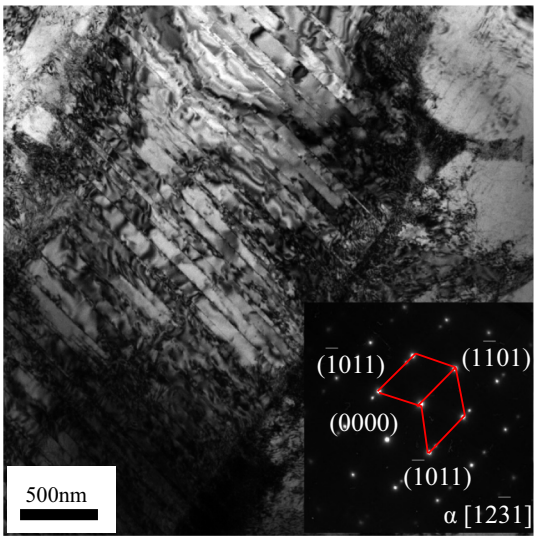

Fig. 9 Alloy matrix presents a deformed twin along [12—31] crystal diffraction

happens in the grain. The stress concentration near the grain boundary provides strong favorable conditions for twin crystal nucleus. The appearance of deformation twins plays a role in stress relief, and can effectively coordinate the plastic deformation of the alloy and make its deformation more uniform.

5 Conclusion

In this paper, different Ge contents were added to LDMed Ti-6Al-4V alloy, and the phase composition and distribution of the obtained alloy were discussed. The microstructure characteristics were observed, the morphology of the lamellar α phase was statistically explained, and the tensile properties of samples were tested. Combined with the matrix characteristics and dislocation morphology, the strengthening mechanism of grain refinement and the second-phase strengthening on the mechanical properties of the alloy is expounded, and the conclusions are as follows.

The addition of Ge improved the overall mechanical properties of LDMed Ti-6Al-4V alloy, and the strength increased with the increase of Ge content. After Ge was added, the growth of coarse columnar crystals was inhibited as the massive phase Ti_5Si_3 was formed. Ge may also promote the matrix lattice structure to produce SRO. The strengthening effects of Ge element alloying on LDMed Ti-6Al-4V alloy are mainly in three aspects. On the millimeter scale, the grain was refined, resulting in fine grain reinforcement. On the micron scale, Ti–Ge compounds are formed, which acts as second-phase strengthening. On the atomic scale, Ge dissolves into the α-Ti matrix, reinforcing the solid solution matrix by forming SRO structure.

Acknowledgements This work was supported by the National Key Research and Development Program of China [Grant No. 2021YFC2801904].

Author contributions CL: writing—review and editing, language modification. JB: writing—original draft, investigation, validation, data curation. XW: reviewing, supervision. GY: supervision, reviewing, editing.

Data availability The data sets generated during and/or analysed during the current study are available from the corresponding authors on reasonable request.

Declarations

Conflict of interest The authors declare that they have no known competing financial interests or personal relationships that could have appeared to influence the work reported in this paper.

References

1. Y. Liu, Z. Qu, B. Wang, Research development and application of Ti6Al4V alloy. Ordnance Mater. Sci. Eng. **28**(1), 47–50 (2007)
2. J. Liu, Microstructure and impact toughness resistance of TC4 titanium alloy. Hot Working Technol. **42**(12), 63–66 (2013)
3. M. Fousová, D. Vojtěch, J. Kubásek, Promising characteristics of gradient porosity Ti-6Al-4V alloy prepared by SLM process. J. Mech. Behav. Biomed. Mater. **69**, 368–376 (2017). https://doi.org/10.1016/j.jmbbm.2017.01.043

4. M. Awd, J. Tenkamp, M. Hirtler, S. Siddique, M. Bambach, Comparison of microstructure and mechanical properties of scalmalloy® produced by selective laser melting and laser metal deposition. Materials **11**, 17 (2018). https://doi.org/10.3390/ma11010017
5. M.H. Loretto, D. Hu, Y.G. Li, Microstructural studies on some ordered Ti-based alloys. Intermetallics **8**, 1243–1249 (2000). https://doi.org/10.1016/S0966-9795(00)00035-2
6. S. Valkov, P. Petrov, R. Lazarova, R. Bezdushnyi, D. Dechev, Formation and characterization of Al–Ti–Nb alloys by electron-beam surface alloying. Appl. Surf. Sci. **389**, 768–774 (2016). https://doi.org/10.1016/j.apsusc.2016.07.170
7. J.C. Han, S.L. Xiao, J. Tian, Y.Y. Chen, L.J. Xu, X.P. Wang, Y. Jia, S.Z. Cao, Microstructure characterization and tensile properties of a Ni-containing TiAl-based alloy with heat treatment. Rare Met. **35**, 26–34 (2016). https://doi.org/10.1007/s12598-015-0626-y
8. A.J. Sterling, B. Torries, N. Shamsaei, S.M. Thompson, D.W. Seely, Fatigue behavior and failure mechanisms of direct laser deposited Ti-6Al-4V. Mater. Sci. Eng. **655**, 100–112 (2016). https://doi.org/10.1016/j.msea.2015.12.026
9. Y. Zhai, D.A. Lados, E.J. Brown, G.N. Vigilante, Fatigue crack growth behavior and microstructural mechanisms in Ti-6Al-4V manufactured by laser engineered net shaping. Int. J. Fatigue **93**, 51–63 (2016). https://doi.org/10.1016/j.ijfatigue.2016.08.009
10. H. Huo, Z.Y. Liang, A.F. Zhang, X.X. Zhang, Anisotropy of mechanical properties of laser-cladding-deposited TC4 titanium alloy containing boron. Chin. J. Lasers **46**(12), 1202008 (2019). https://doi.org/10.3788/CJL201946.1202008
11. Z.J. Qi, X.X. Zhang, Y.Y. Wang, H. Huo, H. Wang, J.Z. Zhang, AF Zhang Effect of B on microstructure and tensile properties of laser additive manufactured TC4 alloy. Chin. J. Lasers **47**(6), 0602002 (2020). https://doi.org/10.3788/CJL202047.0602002
12. W. Li, Y. Yang, J. Liu, Y. Zhou, M. Li, S. Wen, Q. Wei, C. Yan, Enhanced nanohardness and new insights into texture evolution and phase transformation of TiAl/TiB2 in-situ metal matrix composites prepared via selective laser melting. Acta Mater. **136**, 90–104 (2017). https://doi.org/10.1016/j.actamat.2017.07.003
13. H.H. Jiang, Z.T. Jiang, Research progress on the effect of rare earth elements on the microstructure and properties of titanium alloys. Powder Metall. Ind. **31**(05), 81–86 (2021)
14. S.L. Yang, T.D. Xu, Q.F. Li, *Materials physics* (Harbin Institute of Technology Press, Harbin, 2003), pp.208–217
15. K.F. Ha, *The microscopic theory of mechanical properties of metals* (Science Press, Beijing, 1983), pp.1–6
16. Y. Wu, F. Zhang, X. Yuan, H. Huang, X. Wen, Short-range ordering and its effects on mechanical properties of high-entropy alloys. J. Mater. Sci. Technol. **62**(03), 214–220 (2021). https://doi.org/10.1016/j.jmst.2020.06.018
17. R. Zhang, S. Zhao, J. Ding, Y. Chong, T. Jia, C. Ophus, Short-range order and its impact on the CrCoNi medium-entropy alloy. Nature **581**, 283–287 (2020). https://doi.org/10.1038/s41586-020-2275-z
18. O.S. Roik, O.M. Yakovenko, V.P. Kazimirov, Formation of short-range order in Al–Ge–Fe melts: influence of composition. Phys. Chem. Liq. **58**(1), 94–104 (2020). https://doi.org/10.1080/00319104.2018.1550776
19. Q.M. Hu, D.S. Xu, D. Li, Ordering in titanium Alloys II: short-range ordering. Acta Metall. Sin. **38**, 565–567 (2002)
20. L.J. Li, Y.Y. Wang, A.F. Zhang, Induction heating assists Si in the study of fine laser cladding deposition of TC4 grains. Chin. J. Lasers **45**(06), 83–88 (2018)
21. P. Åkerfeldt, M.L. Antti, R. Pederson, Influence of microstructure on mechanical properties of laser metal wire-deposited Ti-6Al-4V. Mater. Sci. Eng. A **674**, 428–437 (2016). https://doi.org/10.1016/j.msea.2016.07.038
22. T.A. Jain, C.G. Huang, C.E. Ho, C.R. Kao, Phase relation in the titanium rich region of the Ge–Si–Ti ternary system. Mater. Trans. JIM **40**, 307–313 (1999). https://doi.org/10.2320/matertrans1989.40.30
23. K.S. Suresh, T. Kitashima, Y. Yamabe-Mitarai, Effect of Si and Ge addition on the evolution of microstructure in near alpha titanium alloy. Adv. Mater. Res. **922**, 744–748 (2014). https://doi.org/10.4028/www.scientific.net/AMR.922.744
24. T. Kitashima, K.S. Suresh, Y. Yamabe-Mitarai, Effect of germanium and silicon additions on the mechanical properties of a near-α titanium alloy. Mater. Sci. Eng. A **597**, 212–218 (2014). https://doi.org/10.1016/j.msea.2013.12.099
25. P. Ge, Y.Q. Zhao, L. Zhou, Strengthening mechanism of β titanium alloy. Mater. Rep. **12**(19), 52–55 (2005)
26. R. Zhang, S. Zhao, C. Ophus, Y. Deng, S.J. Vachhani, B. Ozdol, R. Traylor, K.C. Bustillo, J.W. Morris, D.C. Chrzan, M. Asta, Direct imaging of short-range order and its impact on deformation in Ti-6Al. Sci. Adv. **5**(12), 2799 (2019). https://doi.org/10.1126/sciadv.aax2799
27. H.D. Fan, A review on the plastic mechanism of magnesium alloy. Chin. J. Solid Mech. **40**(4), 4–42 (2019)
28. M. Kumar, V.K. Vasudevan, Deformation-induced pseudo-twinning and a new superstructure in Ni2Mo precipitates contained in a Ni-25Mo-8Cr alloy. Acta Mater. **44**(9), 3575–3583 (1996). https://doi.org/10.1016/1359-6454(96)00005-5
29. X.R. Guo, J.J. Shen, Simulation of plastic behavior of Cu crystals induced by twin-induced softening and reinforcement. Acta Metall. Sin. **58**(03), 375–384 (2022). https://doi.org/10.11900/0412.1961.2021.00230